Anchimeric Assistance by Platinum(II) in the Epimerizations of [PtX(CHXSiMe$_3$)(*R*,*R*-chiraphos)]

Roberto Argazzi and Paola Bergamini*

Dipartimento di Chimica dell'Università di Ferrara e Centro di Fotochimica CNR, Via L. Borsari 46, 44100 Ferrara, Italy

Emiliana Costa, Victoria Gee, John K. Hogg, Antonio Martín, A. Guy Orpen, and Paul G. Pringle*

School of Chemistry, University of Bristol, Cantocks Close, Bristol BS8 1TS, U.K.

Received July 17, 1996[⊗]

The crystal structures of solvates of [PtCl(*S*-CHClSiMe$_3$)(*R*,*R*-chiraphos)], [PtBr(*S*-CHBrSiMe$_3$)(*S*,*S*-chiraphos)], and [PtCl(*R*-CHClSiMe$_3$)(*R*,*R*-chiraphos)] (chiraphos = 2,3-bis(diphenylphosphino)butane) have been determined allowing assignment of the absolute stereochemistry for all the species [PtX(CHXSiMe$_3$)(chiraphos)], **1a**−**c** and **2a**−**c** (X = Cl, Br, I). Inversion at the α-carbon in [PtX(CHXSiMe$_3$)(chiraphos)] has been observed at ambient temperature and below for X = Br or I and at elevated temperatures for X = Cl. The rates of these epimerizations have been monitored by ^{31}P NMR spectroscopy (X = Cl or Br) or polarimetry (X = Br or I). All the epimerizations follow first order kinetics and the rate constants k_{obs} have been calculated. From these values the following can be deduced: (i) The rates increase in the order Cl < Br < I. (ii) Addition of large amounts of halide salts has only a small effect on the rate of epimerization. (iii) The reactions are significantly slower in MeCN than in $CHCl_3$ or CH_2Cl_2. A mechanism consistent with these observations is proposed involving α-halogen migration to the platinum(II).

Introduction

We[1] and others[2] have previously shown that N_2-CHSiMe$_3$ reacts with complexes of the type [PtX$_2$(*R*,*R*-chiraphos)] (X = Cl, Br or I) to give [PtX(CHXSiMe$_3$)-(*R*,*R*-chiraphos)], **1a**−**c** and **2a**−**c** (eq 1), often with high

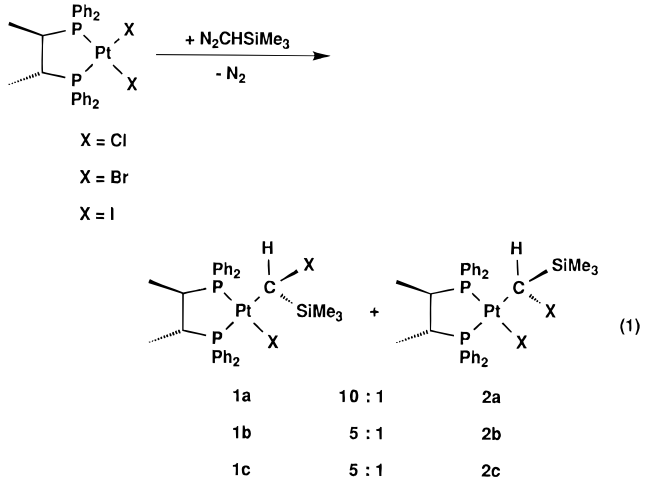

(1)

diastereoselectivity. These compounds may be useful in further syntheses[3] if they are configurationally stable and will undergo substitutions stereospecifically. To address the first of these provisos it was of interest to investigate the factors that control the rate of epimerization at the α-carbon in **1a**−**c** and **2a**−**c**.

Results and Discussion

The chiraphos complexes **1a**−**c** and **2a**−**c** were particularly suitable for the detailed investigation of epimerization because we observed that they epimerized at a measurable rate and moreover the absolute configurations of all the complexes have been determined by X-ray crystallography (see below). The two routes to **1a**−**c** and **2a**−**c** (eqs 1 and 2) yield different proportions of the diastereoisomers. Indeed the pure *RRR*-diastereoisomers, **1a**−**c**, are readily obtained by fractional crystallization of the product from the insertion reaction (eq 1), and samples rich in the *RRS*-diastereoisomers, **2a**, **2b**, are readily separated from the 1:1 mixtures of diastereoisomers obtained via the route shown in eq 2 (see Experimental Section).

Structural Studies. The crystal structures of [PtCl-(*S*-CHClSiMe$_3$)(*R*,*R*-chiraphos)], **2a**, as its diethyl ether solvate (**2a**·OEt$_2$), [PtBr(*S*-CHBrSiMe$_3$)(*S*,*S*-chiraphos)], the enantiomer of **1b**, as its dichloromethane solvate (**1b***·CH_2Cl_2), and [PtI(*R*-CHISiMe$_3$)(*R*,*R*-chiraphos)], **1c**, as its dichloromethane solvate (**1c**·CH_2Cl_2), were determined. Figures 1−3 show the molecular structures of the complexes, and Table 1 gives important structural

[⊗] Abstract published in *Advance ACS Abstracts,* November 15, 1996.

(1) Bergamini, P.; Costa, E.; Orpen, A. G.; Ganter, C.; Pringle, P. G. *J. Chem. Soc., Dalton Trans.* **1994**, 651−655.

(2) McCrindle, R.; McAlees, A. J. *Organometallics* **1993**, *12*, 2445−2461.

(3) (a) Friedrich, H. B.; Moss, J. R. *Adv. Organomet. Chem.* **1991**, *33*, 235. (b) Steinborn, D. *Angew. Chem., Int. Ed. Engl.* **1992**, 401. (c) Kermode, N. J.; Lappert, M. F.; Skelton, B. W.; White, A. H.; Holton, J. *J. Chem. Soc., Chem. Commun.* **1981**, 698. (d) Engelter, C.; Moss, J. R.; Nassimbeni, L. R.; Niven, M. L.; Reid, G.; Spiers, J. C. *J. Organomet. Chem.* **1986**, *315*, 255. (e) Hoover J. F.; Stryker, J. M. *Organometallics* **1988**, *7*, 2082. (f) McCrindle, R.; Arsenault, G. J.; Gupta, A.; Hampden-Smith, M. J.; Rice, R.; McAlees, A. J. *J. Chem. Soc., Dalton Trans.* **1991**, 949. (g) Hoover J. F.; Stryker, J. M. *J. Am. Chem. Soc.* **1989**, *111*, 6466. (h) McCrindle, R.; Ferguson, G.; McAlees, A. J. *J. Chem. Soc., Chem. Commun.* **1990**, 1524. (i) Hoover J. F.; Stryker, J. M. *J. Am. Chem. Soc.* **1990**, *112*, 464. (j) McCrindle, R.; Arsenault, G. J.; Farawaha, R.; Hampden-Smith, M. J.; McAlees, A. J. *J. Chem. Soc., Chem. Commun.* **1986**, 943.

S0276-7333(96)00595-X CCC: $12.00

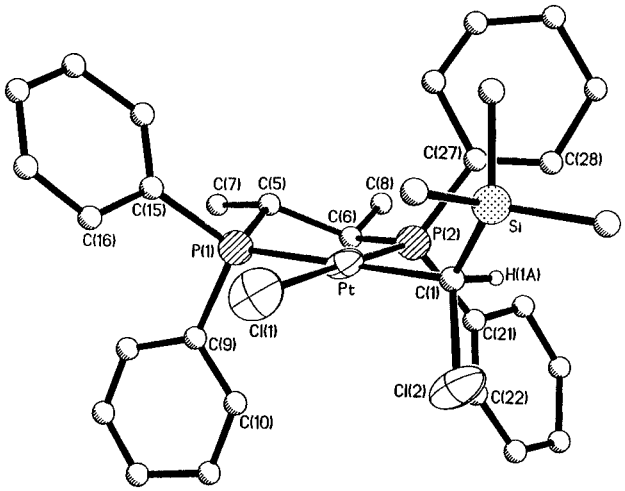

Figure 1. Molecular structure of **2a** showing the labeling scheme. All hydrogen atoms bar H(1a) have been omitted for clarity.

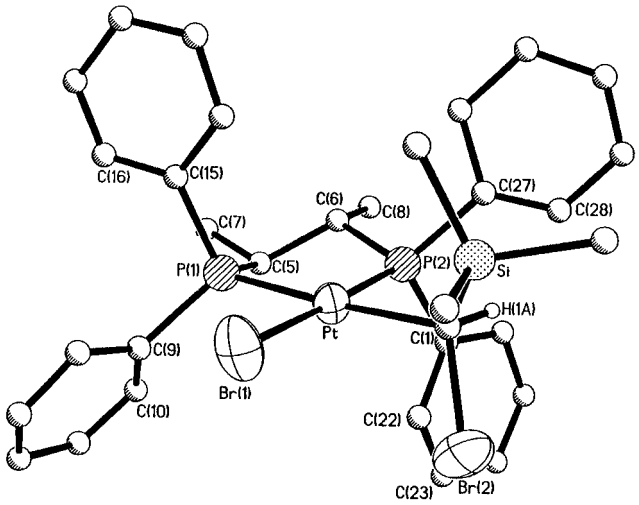

Figure 2. Molecular structure of **1b*** showing the labeling scheme. All hydrogen atoms bar H(1a) have been omitted for clarity.

parameters for these molecules. In each case the structure determination unambiguously confirms the absolute configuration shown, thereby allowing assignment of the stereochemistry of the more stable (for **1b** and **1c**) and less stable (for **2a**) diastereomers formed. In all these structures the same general molecular structure is adopted. Thus in each case the platinum

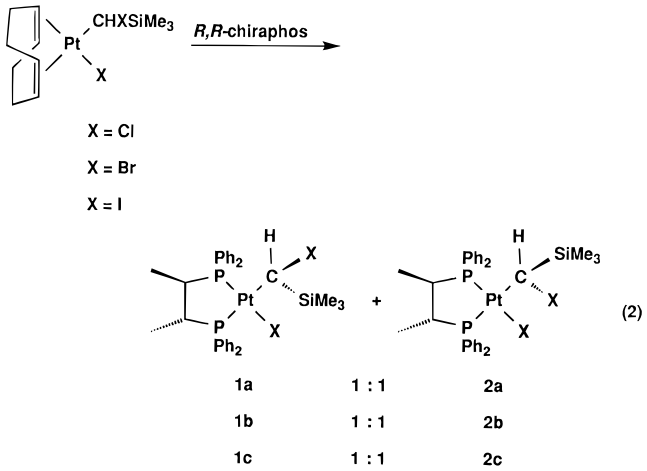

(2)

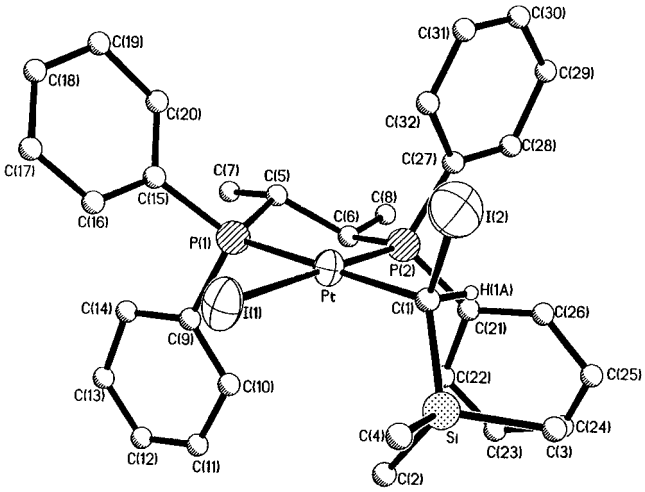

Figure 3. Molecular structure of **1c** showing the labeling scheme. All hydrogen atoms bar H(1a) have been omitted for clarity.

Table 1. Selected Bond Distances (Å), Angles (deg), and Torsion Angles (deg) from the Crystal Structures of 2a·OEt_2, 1b*·CH_2Cl_2, and 1c·CH_2Cl_2

	2a·OEt_2 (X = Cl)	**1b***·CH_2Cl_2 (X = Br)	**1c**·CH_2Cl_2 (X = I)
Pt−P(1) (*trans* to C)	2.299(9)	2.296(7)	2.294(4)
Pt−P(2) (*trans* to X)	2.225(8)	2.209(8)	2.220(2)
Pt−C(1)	2.05(2)	2.15(3)	2.101(9)
Pt−X(1)	2.347(8)	2.492(3)	2.658(1)
C(1)−Pt−P(2)	91.7(10)	90.8(8)	88.7(2)
C(1)−Pt−P(1)	178.2(9)	175.9(9)	174.3(2)
P(2)−Pt−P(1)	86.6(3)	85.8(3)	86.09(9)
C(1)−Pt−X(1)	91.7(10)	90.2(8)	92.8(2)
P(2)−Pt−X(1)	175.6(4)	177.8(2)	177.77(5)
P(1)−Pt−X(1)	90.0(4)	93.2(2)	92.39(8)
P(1)−C(5)−C(6)−P(2)	−41.7	50.4	−52.0
X(1)−Pt−C(1)−X(2)	56.9	69.8	−69.0

is square planar with only small deviations from ideal coordination geometry. The $CHXSiMe_3$ group is oriented so as to place the hydrogen close to the coordination plane and oriented *anti* to the halide ligand (although see below), the chiraphos adopts the usual δ (for **1b***) or λ conformation (for **2a** and **1c**) with both methyl groups in equatorial sites as expected, and the Pt−P distances reflect the higher *trans* influence of the $CHXSiMe_3$ group compared with halide ligands. The relatively poor precision of the structures of **2a**·OEt_2 and **1b***·CH_2Cl_2 preclude more detailed discussion of the molecular geometries.

In the crystal structures of both **1b***·CH_2Cl_2 and **1c**·CH_2Cl_2 (which are isomorphous but of the opposite handedness to one another) there is apparently some "disorder" of the X atom site, to the extent of *ca.* 10% in each case. The minor position is close to the major site (within 1.5 Å in each case) and apparently corresponds to either a rotamer of the main structure or the presence of a small amount of the minor diastereomer cocrystallized with the dominant species in the solid. If the latter is the case then it seems that the crystals studied contain a solid solution of the major and minor diastereomers in the ratio *ca.* 10:1, in which the packing and spatial arrangement of the $PtX(CSiMe_3)$(chiraphos) fragment is essentially identical for both diastereomers with the only variation being in the disposition of the halide and hydrogen atoms bound to C(1). No second

Table 2. ^{31}P NMR Data[a]

	$\delta(P_A)$	$^1J(PtP_A)$	$\delta(P_B)$	$^1J(PtP_B)$	$^2J(P_AP_B)$	ratio[b]
1a	42.92	4034	44.00	1794	13	10
2a	44.35	4116	46.27	1783	13	
1b	43.18	4000	42.27	1818	13	5
2b	45.28	4053	45.44	1812	12	
1c	41.40	3843	38.84	1839	12	5
2c	42.85	3906	42.85	1838	12	

[a] Spectra (81 MHz) measured in MeCN at 21 °C; chemical shifts (δ) in ppm (±0.1) to high frequency of 85% H_3PO_4. Coupling constants (J) in Hz (±3). P_A is trans to the halogen, and P_B is trans to the carbon.

sites were observed for the $SiMe_3$ groups in these structures, in accord with this hypothesis.

The samples of **2a**, **1b***, and **1c** from which the single crystals had been selected for the crystallography were redissolved in $CDCl_3$ at −60 °C (conditions under which epimerization is very slow—see below) and the ^{31}P NMR spectra obtained to confirm that they were the major (**1b***, **1c**) or minor (**2a**) diastereoisomers; the spectra of **1b*** and **1c** obtained thus did indeed show the presence of small quantities (*ca.* 10%) of the diastereoisomers **2b*** and **2c**, as suggested by the crystallography.

Epimerization Studies. It has thus been established that the major product from the reaction of N_2-$CHSiMe_3$ with [PtX_2(*R*,*R*-chiraphos)] (eq 1) has an *R*-configuration at the α-carbon. ^{31}P NMR spectroscopy is a convenient method for following the epimerization of the diastereoisomers **1a**−**c** and **2a**−**c** because the signals are characteristic and clearly distinguished (see Table 2). Integration of the spectra for strictly 1:1 mixtures of the diastereoisomers, obtained *in situ* by the route shown in eq 2, confirmed the validity of using integration of the ^{31}P NMR signals as a measure of relative concentrations. The main drawback with NMR for determining the rates is that each spectrum required at least 3 min to accumulate, incurring large errors in the measurements for the more rapid epimerizations. In such cases, polarimetry was used to follow the kinetics. The data were all analyzed according to the following expression (see Experimental Section for details of the analysis and Supporting Information for all the plots):

$$\text{rate} = k_{obs}[\text{Pt}] + \text{constant} \qquad k_{obs} = k_1 + k_{-1}$$

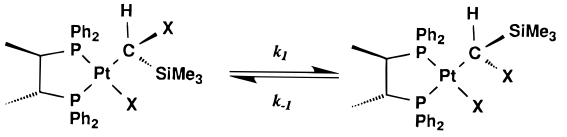

1a 1b 1c 2a 2b 2c (3)

We found that epimerization of the dichloro complexes **1a** and **2a** is detectable by ^{31}P NMR spectroscopy only at high temperatures. The dichloro complexes **1a** and **2a** are configurationally stable under ambient conditions since no epimerization of the dichloro complexes **1a** and **2a** was detected over 14 d in MeCN or $CDCl_3$ at +20 °C. In refluxing $CDCl_3$, solutions that were initially pure **1a** or pure **2a** had both become invariant *ca.* 3:1 mixtures of **1a** and **2a** after 4 days. The proportions in these final solutions indicate that the equilibrium constant for eq 3 (X = Cl) is *ca.* 3 at +61 °C in $CDCl_3$. The epimerization obeys first order kinetics with k_{obs} (334 K) of the order of 10^{-6} s^{-1}. The rate of equilibration of **2a** in the polar, coordinating solvent MeCN at +61 °C was less than that in $CDCl_3$ at the same temperature (see Table 3).[4] Adding Cl^- did not noticeably affect the rate of equilibration of **1a** and **2a** in $CDCl_3$ or MeCN (see Table 3).

In $CDCl_3$ the dibromo complexes **1b** and **2b** epimerize more rapidly than the dichloro analogues. Thus solutions of pure dibromide **1b** or pure **2b** epimerized to 5:1 mixtures of diastereoisomers over 24 h at +20 °C. The epimerization, which was followed by ^{31}P NMR spectroscopy and polarimetry, followed first-order kinetics with k_{obs} (at 293 K) of the order of 10^{-4} s^{-1}. The rate shows a strong solvent dependence: compared to $CHCl_3$, k_{obs} is a factor of 10 smaller in MeCN and a factor of 10 larger in CH_2Cl_2. Added bromide (up to 0.5 M NaBr in MeCN or 0.4 M Pr_4NBr in $CHCl_3$) increased the rate of epimerization but by a smaller factor than increasing the polarity of the solvent from $CHCl_3$ to CH_2Cl_2 (see Table 3).

The iodides **1c** and **2c** epimerized too quickly to be followed by ^{31}P NMR spectroscopy. However the rates of equilibration of 1:1 mixtures of the diiodides **1c** and **2c**, generated *in situ* (see Experimental Section), were accurately measured by polarimetry. The equilibration followed first order kinetics with k_{obs} (at 293 K) of the order of 10^{-3} s^{-1}. As shown in Table 3, the effect of added iodide on the rate of equilibration is small and of the same order as the effect of the solvent; k_{obs} increases in the order MeCN < CH_2Cl_2 < $CDCl_3$.

The lability of the dibromo and diiodo systems made it possible to carry out variable-temperature studies of the equilibria from which the thermodynamic functions have been estimated (see Experimental Section). In both cases the conclusion is that the diastereoisomers are separated by very little in enthalpy (*ca.* −10 kJ mol^{-1} at 298 K) and the solvent ($CDCl_3$, MeCN, CH_2Cl_2) has little effect on the equilibrium constants.

Mechanistic Hypothesis. Inversion of configuration at tetrahedral halocarbons has been a topic for mechanistic investigations for over 100 years.[5] Two generally accepted limiting mechanisms are as follows: (i) loss of halogen as ionic halide and formation of a planar carbonium ion—evidence for this mechanism includes first-order kinetics and acceleration by polar solvents; (ii) nucleophilic attack by external halide—evidence for this mechanism includes second-order kinetics. We have shown that the inversions at the α-carbons in **1a**−**c** and **2a**−**c** follow first-order kinetics but are not accelerated by polar solvents showing that neither of the classical mechanisms is operating.

The α-halogen migration mechanism shown in Scheme 1 is consistent with our observations on the epimerizations of **1a**−**c** and **2a**−**c**. The five-coordinate carbene complex **A** is formed by migration of a halogen from carbon to platinum via square-pyramidal intermediates

(4) The kinetic measurements at high temperatures in $CHCl_3$ and CH_3CN were complicated by some decomposition to [$PtCl_2$(*R*,*R*-chiraphos)]. The less stable isomer **2a** decomposes more rapidly than **1a**, and after 24 h, samples that were initially pure **2a** had decomposed to the following extent: in MeCN at 65 °C, 28 mol % (8 mol % in the presence of 0.13 M LiCl); in $CHCl_3$ at 61 °C, 11 mol % (7 mol % in the presence of 0.15 M [NBu_4]Cl). The k_{obs} values given in Table 3 have larger errors than the others.

(5) March, J. In *Advanced Organic Chemistry*, 4th ed.; John Wiley & Sons: New York, 1992; Chapter 10.

Table 3. Kinetic and Thermodynamic Data[a]

complexes	solvent	[X⁻]/M	method	*T*/°C	k_{obs}/ s^{-1}	$t_{1/2}$[b]	*K*[c]
1a/2a[d]	$CDCl_3$	0	NMR	61	10×10^{-6}	20 h	3
	$CDCl_3$	0.17[e]	NMR	61	11×10^{-6}	20 h	
	CD_3CN	0	NMR	61	2.7×10^{-6}	70 h	
	CD_3CN	0.17[e]	NMR	61	2.5×10^{-6}	80 h	
1b/2b	$CDCl_3$	0	NMR	20	1.1×10^{-4}	100 min	5
	$CHCl_3$		polarimetry		1.5×10^{-4}	75 min	
	$CHCl_3$	0.4[f]	polarimetry	20	3.6×10^{-4}	32 min	
	CH_2Cl_2	0	polarimetry	20	9.0×10^{-4}	13 min	5
	CD_3CN	0	NMR	20	9.0×10^{-6}	21 h	5
	CD_3CN	0.5[g]	NMR	20	15×10^{-6}	13 h	
1c/2c	$CHCl_3$	0	polarimetry	20	3.9×10^{-3}	3 min	5
	$CHCl_3$	0.3[h]	polarimetry	20	8.9×10^{-3}	1 min	
	CH_2Cl_2	0	polarimetry	20	3.0×10^{-3}	4 min	5
	CH_3CN	0	polarimetry	20	2.2×10^{-3}	5 min	5
	CH_3CN	0.3[i]	polarimetry	20	1.2×10^{-3}	10 min	

[a] See the Experimental Section for the methods employed and Supporting Information for the individual measurements. The estimated accuracy of the k_{obs} determinations depends on whether the method was integration of NMR spectra (10−20%) or polarimetry (<5%). [b] ln 2/k_{obs}. [c] Equilibrium constant at given temperature and solvent. [d] The data for **1a/2a** are prone to large errors because of the few number of data points (see Supporting Information) used and the complication associated with some decomposition (see ref 4). [e] Bu^n_4NCl. [f] Et_4NBr. [g] LiBr. [h] Pr^n_4NI. [i] NaI.

Scheme 1. Proposed Mechanism for the Epimerization and Insertion Reactions (Phenyl Groups on Phosphorus Removed for Clarity).

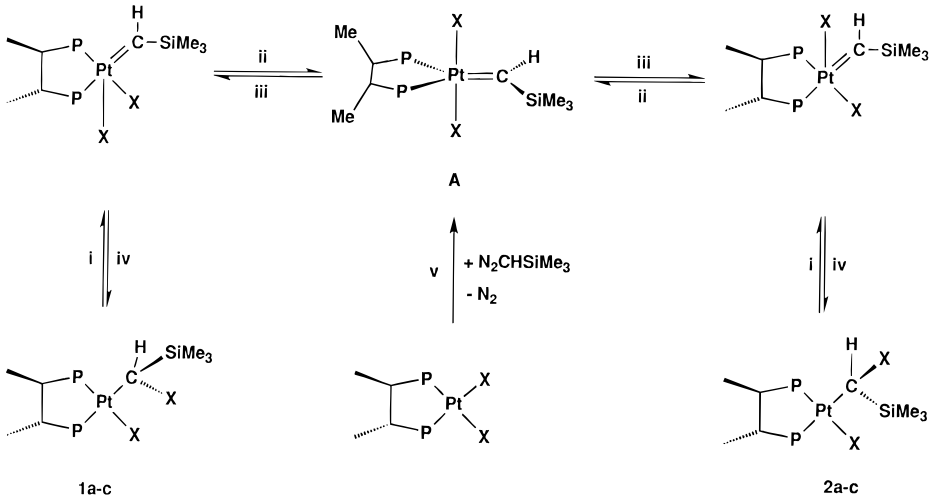

(steps i and ii).[6] The migration of one or other of the halides in **A** back to carbon (steps iii and iv) would give the two different diastereoisomers. If step i is rate determining and is viewed as a C−X oxidative addition, it is readily understood why the rate of epimerization is in the order I > Br > Cl. This intramolecular rearrangement mechanism via neutral intermediates also explains why the rate of epimerization is essentially independent of added halide and why solvent polarity has little effect on the rates. The observed inhibition of the epimerization of the chloro, bromo, and iodo complexes by MeCN may be a consequence of occupation of the axial sites on platinum by the strongly solvating MeCN.

The reactions of $[PtX_2(chiraphos)]$ (X = Cl, Br, and I) with $N_2CHSiMe_3$ always give the thermodynamic mixtures of diastereomeric products.[1,2] From the kinetic results described here for the dibromo and diiodo complexes, it could be argued that the products initially formed may not be at equilibrium and they then epimerize under the reaction conditions. However such an explanation can be excluded for why the chloro complexes **1a** and **2a** are also formed as an equilibrium (3:1) mixture when $[PtCl_2(chiraphos)]$ reacts with $N_2CHSiMe_3$ at +61 °C, since under these conditions epimerization is very slow (see Table 3). It is possible to rationalize why all of these insertion reactions give the thermodynamic mixture of products if they also go via **A** (step v in Scheme 1) and then the ratio of the rates **A** → **1a**−**c** and **A** → **2a**−**c** are equal to the equilibrium constants *K*. We therefore propose the unified mechanism for epimerization and insertion shown in Scheme 1.[6]

Conclusion. We have shown that the configurational stability of complexes of the type $[PtX(CHXSiMe_3)(R,R\text{-chiraphos})]$ decreases in the order X = Cl > Br > I and suggest that the kinetics support a platinum(II)-mediated mechanism for the epimerization involving α-halogen migration.

Experimental Section

All the reactions and experiments were carried out in air except where specified otherwise. *R,R*-chiraphos, *S,S*-chiraphos, and $N_2CHSiMe_3$ (2 M in *n*-hexane) were used as

(6) As one reviewer suggested, a mechanism based entirely on square-pyramidal intermediates can also explain the epimerizations and indeed a mechanism for the insertions of $CHSiMe_3$ into Pt−Cl bonds invoking only square pyramidal intermediates was recently discussed in detail by McCrindle and McAlees (see ref 2).

purchased (Aldrich) . [PtX$_2$(*R,R*-chiraphos)] and [PtX(CHXSiMe$_3$)(cod)], X = Cl, Br, or I (cod = 1,5-cyclooctadiene), were made as previously described.[1] We have previously reported ^{1}H, ^{31}P NMR, and elemental analytical data for all of the complexes **1a**−**c** and **2a**−**c** as mixtures of diastereoisomers.[1] The purity of all the samples used in the kinetic measurements was checked by ^{31}P and ^{1}H NMR spectroscopy. Polarimetric measurements were performed on a Perkin Elmer 241 at 25 °C.

Preparation of a 1:1 Mixture of [PtCl(*R*-CHClSiMe$_3$)(*R,R*-chiraphos)] (1a) and [PtCl(*S*-CHClSiMe$_3$)(*R,R*-chiraphos)] (2a). A 50 mg amount of *R,R*-chiraphos (0.12 mmol) was dissolved in 5 mL of CH_2Cl_2 and added dropwise over 5 min under nitrogen to a solution of 54 mg (0.12 mmol) of [PtCl(CHClSiMe$_3$)(cod)] in 5 mL of CH_2Cl_2. The solution was stirred for 1 h and then the solvent removed under vacuum to give a white solid, 88 mg, 94%, which was washed with 3 × 5 mL of *n*-hexane. A 1:1 mixture of **1b** and **2b** was obtained in a similar way from [PtBr(CHBrSiMe$_3$)(cod)] in 89% yield.

Preparation of a 10:1 Mixture of [PtCl(*R*-CHClSiMe$_3$)(*R,R*-chiraphos)] (1a) and [PtCl(*S*-CHClSiMe$_3$)(*R,R*-chiraphos)] (2a). A solution of $N_2CHSiMe_3$ (1.5 mL of a 2 M in hexane, 3.0 mmol) was added over 5 min under nitrogen to a suspension of [PtCl$_2$(*R,R*-chiraphos)] (208 mg, 0.30 mmol) in dry CH_2Cl_2 (10 mL). The mixture was stirred for 18 h, and then the volume was reduced to 1 mL under vacuum. Addition of diethyl ether (20 mL) precipitated the white product as a 10:1 mixture of **1a** and **2a**, 222 mg, (95%). Equilibrium mixtures of **1b** and **2b** (74%) and **1c** and **2c** (79%) are obtained similarly from [PtX$_2$(*R,R*-chiraphos)] (X = Br or I).

Preparation of [PtCl(*R*-CHClSiMe$_3$)(*R,R*-chiraphos)] (1a). Complex **1a** was prepared by redissolving the 10:1 equilibrium mixture of **1a** and **2a** (220 mg) in benzene (1 mL) to give a clear solution. After *ca.* 10 min, a white precipitate is formed (**2a**), which was filtered off. The filtrate was reduced to dryness to give 200 mg (90%) of pure **1a**. Occasionally the product obtained still contained traces of **2a**, and in these cases the purification procedure was repeated.

Preparation of [PtCl(*S*-CHClSiMe$_3$)(*R,R*-chiraphos)] (2a). A solution of 95 mg of *R,R*-chiraphos (0.22 mmol) in 15 mL of benzene was added dropwise over 10 min to a solution of 110 mg (0.24 mmol) of [PtCl(CHClSiMe$_3$)(cod)] in 15 mL of benzene with stirring at room temperature under nitrogen. After a further 10 min, the clear reaction mixture was cooled to −14 °C. After 1 h, the frozen solution was allowed to warm to +20 °C to give a white suspension. The solid was filtered off and washed with 3 × 2 mL of benzene to give 65 mg (67%) of pure **2a**. Crystals of **2a** suitable for X-ray crystallography were grown from $CHCl_3$/Et_2O.

Separation of [PtBr(*R*-CHBrSiMe$_3$)(*R,R*-chiraphos)] (1b) and [PtBr(*S*-CHBrSiMe$_3$)(*R,R*-chiraphos)] (2b). A 200 mg amount of crude 1:1 mixture of **1b** and **2b** was added to 7 mL of benzene to give a clear solution. After *ca.* 1 min a white precipitate of **2b** began to form. After 5 min the white solid, which is pure **2b** (100 mg, 100%), was filtered off, washed with 2 × 1 mL of benzene, and dried. The filtrate was reduced to dryness, and the oily residue was triturated with *n*-hexane to give a solid, which was then filtered off and dried; this solid was essentially pure **1b**, 90 mg (90%). Crystals of [PtBr(*S*-CHBrSiMe$_3$)(*S,S*-chiraphos)] (**1b***), the enantiomer of **1b**, suitable for X-ray crystallography were grown from CH_2Cl_2/Et_2O.

Preparation of [PtI(*R*-CHISiMe$_3$)(*R,R*-chiraphos)] (1c). An equilibrium mixture of **1c** and **2c**, obtained as described above, was recrystallized from CH_2Cl_2 and Et_2O to give crystals of **1c** (as shown by ^{31}P NMR spectroscopy at −60 °C) suitable for X-ray crystallography. Note that **2c** was never isolated in pure form because it rapidly epimerizes at ambient temperature.

Epimerization of Chloro Complexes 1a and 2a by ^{31}P NMR Spectroscopy. In a typical experiment, 25 mg of pure **1a**, pure **2a**, or a 1:1 mixture was dissolved in 1 mL (0.032 M) of $CDCl_3$ or CD_3CN and the spectra were recorded at convenient times over several days. Another set of experiments in each solvent were performed at +61 °C. The same experiments were also carried out in the presence of 0.17 M NBu_4Cl.

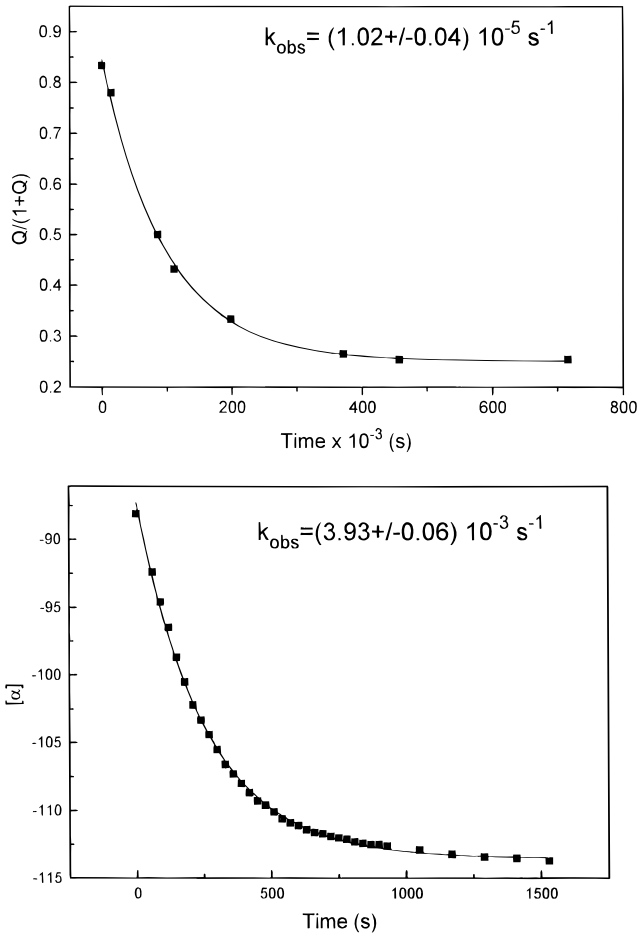

Figure 4. Typical exponential curve fits used for the analysis of the kinetic data: (a, top) NMR data for equilibration of **1a**/**2a** in $CDCl_3$; (b, bottom) polarimetry data for the equilibration of **1c**/**2c** in $CHCl_3$.

Epimerization of Bromo Complexes 1b and 2b by ^{31}P NMR Spectroscopy. A 22 mg amount of **1b**, **2b,** or a 1:1 mixture was dissolved in 1 mL (0.025 M) of $CDCl_3$, CD_2Cl_2, CD_3CN, and the spectra were recorded at intervals over 48 h. In the case of **2b** in CD_3CN the experiments were also performed in the presence of various concentrations of LiBr (0.125, 0.25, 0.375, and 0.5 M).

Epimerization of Bromo Complexes 1b and 2b by Polarimetry. A 20 mg amount of pure **1b**, pure **2b**, or a 1:1 mixture was dissolved in 1 mL of $CHCl_3$ or CH_3CN (0.023 M), and the values of optical rotation were recorded at regular intervals over 8 h.

Epimerization of the Iodo Complexes 1c and 2c by Polarimetry. A 0.020 M solution of a 1:1 mixture of **1c** and **2c** was generated *in situ* by mixing a 0.5 mL solution ($CHCl_3$, CH_3CN or CH_2Cl_2) containing 13.4 mg (0.020 mmol) of [PtI(CHISiMe$_3$)(cod)] with 0.5 mL of a solution of *R,R*-chiraphos (9 mg, 0.020 mmol) in the same solvent. The measurements of optical rotation were then started immediately. Other experiments were performed by replacing the solvent with a 0.3 M solution of NaI in CH_3CN or a 0.3 M solution of NPr_4I in $CHCl_3$.

Kinetic Analysis. (a) NMR. We showed that integration of the ^{31}P NMR signals was valid for determining *Q*, the ratio of the two diastereoisomers—see main text. It can be shown (see Supporting Information) that k_{obs} can be obtained from a

Table 4. Details of Crystal Structure Determinations

	2a·OEt_2	**1b***·CH_2Cl_2	**1c**·CH_2Cl_2
	Crystal Data		
empirical formula	$C_{36}H_{48}Cl_2OP_2PtSi$	$C_{33}H_{40}Br_2Cl_2P_2PtSi$	$C_{33}H_{40}Cl_2I_2P_2PtSi$
M_n	852.76	952.49	1046.47
cryst size (mm)		0.50 × 0.30 × 0.25	0.50 × 0.25 × 0.25
cryst system	orthorhombic	Hexagonal	Hexagonal
space group	$P2_12_12$ (No. 18)	$P6_1$ (No. 169)	$P6_5$ (No. 170)
unit cell dimens			
a (Å)	15.410(13)	11.689(2)	11.731(2)
b (Å)	26.33(3)	11.689(2)	11.731(2)
c (Å)	9.924(10)	46.868(12)	46.85(7) Å
α (deg)	90	90	90
β (deg)	90	90	90
γ (deg)	90	120	120
V (Å^3)	4026(4)	5546(2)	5584(5)
Z	4	6	6
D(calc) (Mg/m^{-3})	1.407	1.711	1.867
abs coeff (mm^{-1})	3.752	6.242	5.711
F(000)	1712	2784	3000
	Data Collection and Reduction		
temp (K)	293(2)	293(2)	173(2)
scan type	Wyckoff, ω	Wyckoff, ω	ω, area detector
index ranges	$0 \le h \le 18$, $0 \le k \le 31$, $0 \le l \le 11$	$0 \le h \le 14$, $0 \le k \le 14$, $-34 \le l \le 56$	$-13 \le h \le 13$, $-13 \le k \le 8$, $-55 \le l \le 54$
reflcns collcd	3999	4762	26400
No. unique reflcns with $I > -3\sigma(I)$	3996	4025	6521
R_{int}	0.00	0.0495	0.0348
reflcns with $I > 2\sigma(I)$	2807	3043	6488
no. azimuthal scan data	576	312	12 298
min, max transm coeffs	0.162, 0.262	0.272, 0.321	0.461,0.764
	Solution and Refinement		
least-squares variables	353	377	377
least-squares restraints	0	1	1
a, b	0.10, 0	0.05,0.0	0.03, 0.0
non-H atoms			
thermal params aniso	all bar solvent atoms	all	all
thermal params iso	solvent atoms	none	none
disorder	solvent atoms	Br(2), Br(2′): 0.92(1):0.08(1)	I(2), I(2′); 0.90(1):0.10(1)
absolute struct param	0.01(4)	−0.01(2)	0.018(5)
final R indices[a]	$R1 = 0.101$, w$R2 = 0.236$	$R1 = 0.070$, w$R2 = 0.154$	$R1 = 0.033$, w$R2 = 0.0912$
goodness-of-fit, S[a]	1.462	1.713	2.130
E_{max}, E_{min} (e Å^{-3})	3.51,−4.50	1.07, −1.37	0.86, −1.59

[a] Residuals calculated for reflections with $I > 2\sigma(I)$; w$R2 = [\sum w\Delta^2/\sum wF_o^4]^{0.5}$; $S = [\sum w\Delta^2/(N - NV)]^{0.5}$; $R1 = \sum||F_o| - |F_c||/\sum|F_o|$; $\Delta = F_o^2 - F_c^2$; N = NO + restraints; $\sigma_c^2(F_o^2)$ = variance in F_o^2 due to counting statistics, $P = [\max(F_o^2,0) + 2F_c^2]/3$.

fitting of an exponential function to a plot of $Q/(1 + Q)$ against time, t. All of the plots are deposited in the Supporting Information, and an example is shown in Figure 4; estimated errors are of the order of 10−20%.

(b) Polarimetry. It can be shown (see Supporting Information) that k_{obs} can be obtained from a fitting of an exponential function to a plot of specific rotation [α] against time, t. All of the plots are deposited in the Supporting Information, and an example is shown in Figure 4; due to the better accuracy of the polarimetric measurements and the larger number of experimental points for each data set, the estimated errors (<5%) are lower than in the NMR experiments.

Estimate of Thermodynamic Functions for the 1b/2b and 1c/2c Equilibria. Solutions of dibromides **1b**/**2b** (40 mg) in 0.4 mL of $CDCl_3$ or $C_2H_2Cl_4$ were allowed to reach equilibrium (as shown by invariant spectra) and the ^{31}P NMR spectra integrated in order to determine the equilibrium constant K: at 322 K, $K = 14$ (equilibrium reached after 2 h); at 298 K, $K = 10$ (equilibrium reached after 2 days); at 263 K, $K = 4$ (equilibrium reached after 3 weeks). A plot of ln K against $1/T$ yielded $\Delta H° -10(\pm1)$ kJ mol^{-1} and $\Delta S° -20(\pm4)$ J mol^{-1} K^{-1}. Similar equilibrium studies for the diiodides **1c**/**2c** yielded the following data (equilibrium was reached in less than 2 h in each case) at specified temperatures: 336 K, $K = 3.8$; 323 K, $K = 4.0$; 310 K, $K = 5.2$; 298 K, $K = 5.6$; 246 K, $K = 10.8$. These data yielded $\Delta H° = -8.0(\pm0.8)$ kJ mol^{-1} and $\Delta S° = -13(\pm3)$ J mol^{-1} K^{-1}.

Structure Determinations of 2a·OEt_2, 1b*·CH_2Cl_2, and 1c·CH_2Cl_2. Many of the details of the structure analyses are listed in Table 4. X-ray diffraction measurements on single crystals mounted in thin-walled glass capillaries for **2a**·OEt_2 and **1b***·CH_2Cl_2 and on a glass fiber under a coating of frozen oil for **1c**·CH_2Cl_2 were made with graphite-monochromated Mo Kα X-radiation ($\bar{\lambda} = 0.710\ 73$ Å) using Siemens four-circle R3m (**2a**·OEt_2, **1b***·CH_2Cl_2) or SMART (**1c**·CH_2Cl_2) diffractometers. In the first two cases crystal quality was considerably less than optimum with relatively weak diffraction observed and poor crystallinity especially for **2a***·OEt_2. Samples chosen for study were the best of many assessed. Intensity data were collected for $2\theta < 50.0°$ by conventional methods for **2a**·OEt_2 and **1b***·CH_2Cl_2 and for **1c**·CH_2Cl_2 by 0.3° width ω steps accumulating area detector frames spanning a hemisphere of reciprocal space. Data were corrected for Lorentz, polarization, long-term intensity fluctuations, and absorption effects on the basis of azimuthal scan data. The structures were solved by direct methods and refined by full-matrix least-squares against F^2 against all data with $I > -3\sigma(I)$ with weights, w, set equal to $[\sigma_c^2(F_o^2) + (aP)^2 + bP]^{-1}$, where $P = [\max(F_o^2,0) + 2F_c^2]/3$ and a and b were assigned values given in Table 4. All non-hydrogen atoms were refined without positional constraints and assigned anisotropic displacement parameters except for the solvent atoms of **2a**·OEt_2. All hydrogen atoms were assigned isotropic displacement parameters and were constrained to ideal geometries. Final difference syntheses showed no chemically significant features, the largest being close to the metal or solvent atoms. In the case of **2a**·OEt_2 the large residual features and high R factors are apparently the result of poor crystal quality which was reflected in the

rocking curves which in turn led to poor integration of intensities. In **1b***·CH_2Cl_2 and **1c**·CH_2Cl_2 a low occupancy (*ca.* 10%) halide atom position bonded to C(1) was observed and refined. In each case the absolute structure was confirmed by refinement of the Flack parameter.[7] Refinements converged to residuals given in Table 4. Complete atomic coordinates, thermal parameters, and bond distances and angles have been included in the Supporting Information. All calculations were made with programs of the SHELXTL-PLUS system.[8] Complex neutral-atom scattering factors were taken from ref 9.

Acknowledgment. We thank the EPSRC for Research Studentships (to J.K.H. and V.G.), a Research Assistantship (to E.C.), and funds to purchase an X-ray diffractometer, Ciba-Geigy for a Senior Research Fellowship (P.G.P.), NATO for a travel grant, and Johnson-Matthey for a loan of platinum salts. One of us (A.M.) thanks the Spanish Ministerio de Educacion y Ciencia for an FPU (Becas en el extranjero) grant.

Supporting Information Available: Tables giving additional details of the X-ray studies, additional bond distances and angles, anisotropic thermal parameters, and complete atom coordinates and *U* values for **2a**, **1b***, and **1c** and text giving details of the kinetic analysis of the NMR and polarimetric data and plots of the exponential fits (36 pages). Ordering information is given on any current masthead page.

OM9605950

(7) Bernardinelli, G.; Flack, H. D. *Acta Crystallogr., Sect. A* **1985**, *A41*, 500.
(8) Sheldrick, G. M. SHELXTL-PLUS Rev. 5, Göttingen, FRG, 1995.
(9) *International Tables for Crystallography*; Kluwer: Dordrecht, The Netherlands, 1992; Vol. C.